Atomistic study of misfit dislocation in metal/SiC(111) interfaces

2010 J. Phys.: Condens. Matter 22 135009

(http://iopscience.iop.org/0953-8984/22/13/135009)

IOP Publishing Journal of Physics: Condensed Matter

J. Phys.: Condens. Matter **22** (2010) 135009 (10pp) doi:10.1088/0953-8984/22/13/135009

Atomistic study of misfit dislocation in metal/SiC(111) interfaces

Yudong Wang[1] **and Nanxian Chen**[1,2]

[1] Department of Physics, Tsinghua University, Beijing 100084, People's Republic of China
[2] Institute for Applied Physics, University of Science and Technology, Beijing 100083, People's Republic of China

E-mail: wangyd05@mails.tsinghua.edu.cn

Received 10 October 2009, in final form 24 February 2010
Published 17 March 2010
Online at stacks.iop.org/JPhysCM/22/135009

Abstract

The interatomic potentials across metal/SiC(111) interfaces are derived from *ab initio* adhesive energies by an inversion method. We use these potentials to investigate the structures, energies and Burgers vectors of misfit dislocations in metal/SiC(111) interfaces. Two kinds of interfacial dislocations are found in M/SiC(111) (M = Au, Ag, Al, Pt) interfaces, where the M/SiC(111) (M = Au, Al) system has partial dislocations and the M/SiC(111) (M = Ag, Pt) system has perfect dislocations. The former has a coherent interface while the latter corresponds to a semi-coherent interface.

(Some figures in this article are in colour only in the electronic version)

1. Introduction

Silicon carbide (SiC), as one of the most promising semiconductors for high-temperature, high-frequency and high-power application, is attracting more and more attention for its wide band gap and excellent performance. In device manufacture, the metal/SiC interface is an essential issue for its key role in determining the properties of the devices. By using different metals, the metal–SiC junction can be either Ohmic or Schottky contact [1]. Furthermore, the electronic properties of metal/SiC interfaces are not only dependent on the type of metal atom, but also on the atomic arrangement near the interface [2, 3]. However, it is difficult in experiment to determine this arrangement, thus theoretical study is needed.

In fact, there have been many *ab initio* calculations concentrating on the electronic properties for the metal/SiC interface [4–6]. Considering the large computational cost in dealing with complex atomic models as well as dynamic processes, some researchers pay attention to interatomic potentials instead [7, 8]. In the present work, we derive interatomic potentials from *ab initio* calculations [9–11] by using the Chen–Möbius inversion method. Note that in most previous works potentials are derived from the properties in the lowest energy state, while in this work we obtain interatomic potentials across the ideal interface model from a series of *ab initio* calculations of stable, metastable or even unstable structures. This method is useful for studying interfacial structures and their dynamic processes.

In a heterogeneous interface, lattice misfit induces misfit dislocations or sometimes dislocation networks [12–15], which may affect interfacial mechanical, optical and electronic properties. For example, atoms in the dislocation core usually occupy high energy states, and the others occupy low energy states. The chemical bonds as well as energy gaps in the dislocation core may change significantly. Therefore, misfit dislocation is an important factor for interfacial structures. Research on this topic is valuable to interface science.

To study interfacial misfit dislocation, we select four typical metals (Au, Ag, Al, Pt) to form interfaces with the SiC(111) surface. The interfacial orientation relationship focused on in this work is metal(111)/SiC(111). The interfacial mismatch is defined as $\gamma = (a_M - a_{SiC})/a_{SiC}$, where a_M and a_{SiC} are the lattice constants of bulk metal and SiC respectively (see table 1). For large-mismatch metals such as Cu and Ni, it is not reliable to use the same dislocation models as Pt, Au, Ag and Al.

The following work includes three parts. First, in section 2, we demonstrate the inversion method to get the required interatomic potentials. Second, in section 3, the structural properties of misfit dislocations in M/SiC(111) (M = Au, Ag, Al, Pt) interfaces are studied. Finally, section 4 contains the conclusion and discussion.

Table 1. Lattice constants and mismatches of M(111)/SiC(111) interfaces (M = Au, Ag, Al, Pt, Cu and Ni).

M	Au	Ag	Al	Pt	Cu	Ni	SiC
a_M or a_{SiC} (Å)	4.0783	4.0857	4.0495	3.9239	3.6147	3.5240	4.3480
γ	−6.3%	−6.0%	−9.3%	−9.8%	−16.9%	−19.0%	—

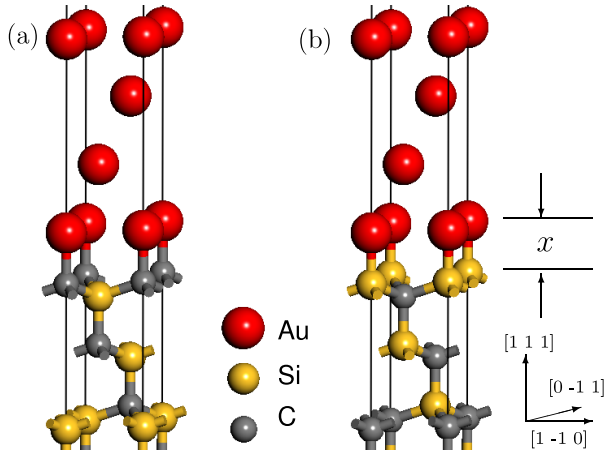

Figure 1. Ideal Au(111)/SiC(111) interface models used for the inversion method. (a) C-terminated, (b) Si-terminated. Each model consists of six metal layers, six Si layers and six C layers. Only a few layers near the interface are presented.

2. Potentials

2.1. Two-body term

A combination of two-body and three-body potentials is assigned for the metal/SiC(111) interface. The former is the main part and is derived by the Chen–Möbius inversion method, while the latter is treated as the modification of the former according to interfacial adhesive energy (AE) curves.

Now, let us introduce the inversion method to get the two-body potentials. This method has been successfully applied in bulk materials such as metals, intermetallic compounds, semiconductors, ionic crystals [16–20], and interface systems such as metal/MgO [21, 22] and metal/Al_2O_3 [23, 24]. Here, we use it to get a series of potentials for metal(111)/SiC(111) interfaces.

The lattice inversion method derives parameter-free interfacial pair potentials from original *ab initio* AEs. For this purpose, the C-terminated and Si-terminated interfaces are considered respectively, with the models shown in figure 1. The interfacial AE (E^{ad}) is defined as

$$E^{ad} = E^{tt} - E^{SiC} - E^{M}, \tag{1}$$

where E^{tt}, E^{SiC} and E^{M} are the total energies of the interface system, isolated SiC slab and metal slab, respectively.

AE is equal to the summation of pair potentials across the interface:

$$E^{ad} = \sum_{ij} \phi_{ij}(r_{ij}), \tag{2}$$

where ij denotes the atom pair across the interface, r_{ij} denotes the atomic distance and ϕ_{ij} denotes the pair potential. Here, atom pairs are M–Si and M–C (M = Al, Au, Ag and Pt in this work). So the AEs (E^{ad}) of C-terminated and Si-terminated interfaces are

$$\begin{aligned} E^{ad}_{C}(x) &= \sum_k a_k \phi_{C-M}(r_k(x)) + \sum_k b_k \phi_{Si-M}(r_k(x)), \\ E^{ad}_{Si}(x) &= \sum_k b_k \phi_{C-M}(r_k(x)) + \sum_k a_k \phi_{Si-M}(r_k(x)), \end{aligned} \tag{3}$$

where x is the interfacial distance, k is the index of C–M and Si–M pairs, $r_k(x)$ is the atomic distance, a_k and b_k are the coordination numbers, and ϕ_{C-M} and ϕ_{Si-M} are the pair interactions. Note that a_k and b_k are based on the symmetry remaining in the metal and SiC slabs.

To simplify the energy expression, we introduce some intermediate variables:

$$\begin{aligned} E_\pm = E^{ad}_C \pm E^{ad}_{Si}, \qquad \phi_\pm = \phi_{C-M} \pm \phi_{Si-M}, \\ c^\pm_k = a_k \pm b_k. \end{aligned} \tag{4}$$

Then (3) is rewritten as

$$E_\pm(x) = \sum_k c^\pm_k \phi_\pm(r_k(x)). \tag{5}$$

To get $\phi_\pm$ from $E_\pm$, we equally divide the range of r into N intervals, which are $d_0 < d_1 < d_2 < \cdots < d_N$. For $r_k(x)$ in (5), we can find an index number n satisfying $d_n \leqslant r_k(x) < d_{n+1}$. By interpolation, $\phi_\pm(r_k(x))$ is approximately equal to

$$\phi_\pm(r_k(x)) = \frac{d_{n+1} - r_k(x)}{d_{n+1} - d_n}\phi_\pm(d_n) + \frac{r_k(x) - d_n}{d_{n+1} - d_n}\phi_\pm(d_{n+1}). \tag{6}$$

Then, we choose a series of interfacial distance values x_1, $x_2, \ldots, x_N$. At x_m, AE is

$$E_\pm(x_m) = \sum_{n=1}^{N} h^\pm_{mn}\phi_\pm(d_n), \tag{7}$$

where coefficients $\{h^\pm_{mn}\}$ are obtained by substituting (6) into (5). In matrix form, $E_\pm = [E_\pm(x_1), E_\pm(x_2), \ldots, E_\pm(x_N)]$ and $\phi_\pm = [\phi_\pm(d_1), \phi_\pm(d_2), \ldots, \phi_\pm(d_N)]$. As a result, (7) is rewritten as

$$E_\pm = \phi_\pm H_\pm. \tag{8}$$

The matrix element of $H_\pm$ is

$$H_{\pm,mn} = h^\pm_{nm}. \tag{9}$$

So

$$\phi_\pm = E_\pm H^{-1}_\pm. \tag{10}$$

Finally, ϕ_{C-M} and ϕ_{Si-M} are obtained by:

$$\phi_{C-M} = \tfrac{1}{2}(\phi_+ + \phi_-) \qquad \phi_{Si-M} = \tfrac{1}{2}(\phi_+ - \phi_-). \tag{11}$$

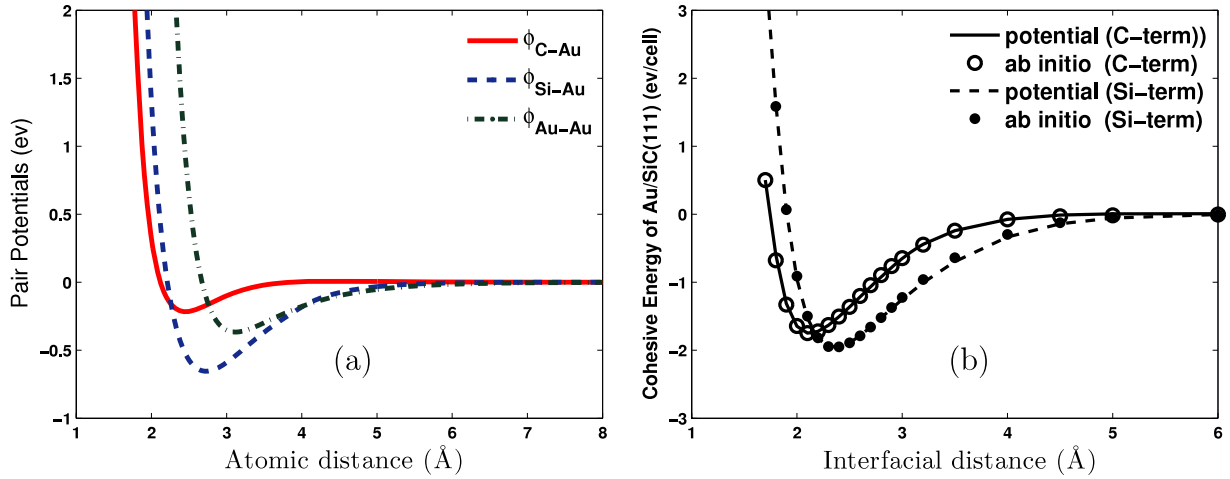

Figure 2. Pair potential (a) and AE (b) curves of the Au/SiC(111) interface. Here $\phi_{\mathrm{Au-Au}}$ for bulk Au is also presented as it will be used in the metal slab. In (b), scattered symbols denote the *ab initio* results, and lines denote pair-potential-calculated results.

Table 2. Two-body potential parameters for metal(111)/SiC(111) interfaces.

	$\phi_{\mathrm{Au-C}}$	$\phi_{\mathrm{Au-Si}}$	$\phi_{\mathrm{Ag-C}}$	$\phi_{\mathrm{Ag-Si}}$	$\phi_{\mathrm{Pt-C}}$	$\phi_{\mathrm{Pt-Si}}$	$\phi_{\mathrm{Al-C}}$ [10]	$\phi_{\mathrm{Al-Si}}$ [10]
D_0 (eV)	20.0959	30.0401	20.2023	30.1051	21.2815	30.2722	0.1392	68.4853
R_0 (Å)	1.0000	1.0000	1.0000	1.0000	1.0000	1.0000	1.0000	1.0000
y	2.0784	1.3763	2.0358	1.3588	2.6728	1.5170	5.7526	1.2844
a_1 (eV)	2.4716	−0.0330	1.2585	0.0054	7.7074	−0.2374	66.9374	75.0606
b_1 (Å^{-1})	10.9813	9.2316	12.8937	9.6162	8.1985	3.4732	5.7654	2.9238
c_1 (Å)	1.7318	3.9789	1.7386	4.0720	1.5418	4.0549	0.9401	0.9512
a_2 (eV)	−6.9938	−14.7021	−6.9290	−14.6264	−7.0506	−14.7741	1.1365	−12.2142
b_2 (Å^{-1})	2.0705	1.4725	1.9743	1.4300	2.0590	1.5953	8.2083	3.6486
c_2 (Å)	1.8643	1.9144	1.8758	1.8660	1.6342	1.8372	1.6578	1.6732
a_3 (eV)	3.3455	7.0814	3.3737	4.3918	3.3618	11.3124	−0.6407	−55.5837
b_3 (Å^{-1})	1.4406	7.9455	1.4554	8.1147	1.5500	6.2888	2.3362	1.3456
c_3 (Å)	1.0634	1.7157	1.0779	1.7515	0.9233	1.6075	2.7657	1.4086

Based on the above method, we can get the two-body potentials of the metal/SiC(111) interfaces from the *ab initio* calculated AEs. Figure 1 shows the interface models used in the *ab initio* calculations. Each model consists of six metal monolayers (MLs) and twelve SiC MLs. The unit cell parameters are chosen as (3.075 Å, 3.075 Å, $x+37.734$ Å, 90°, 90°, 60°). For this ideal interface model, the metal lattice is forced to fit the SiC lattice, since deformation is much easier in metal lattice than in SiC. The vacuum gap is chosen to be 12 Å. We perform a series of calculations to obtain the AE curves by varying the interfacial distance x from 1 to 8 Å. The metal and SiC slabs are always kept as rigid bodies during the elongation of x. This will help simplify the inversion procedure since the method is based on the partial bulk symmetries remaining in metal and SiC slabs.

The *ab initio* calculations, based on the density functional theory (DFT), are performed by the CASTEP program [25–27] with the generalized gradient approximation and Perdew–Wang 1991 exchange correlation functional (GGA-PW91). Ultra-soft pseudopotentials are used. The k-points mesh is $8 \times 8 \times 3$ generated by the Monkhorst–Pack scheme [28, 29]. The plane-wave cutoff energy is chosen as 400 eV and the energy tolerance is 2×10^{-6} eV/atom.

Figure 2 shows the resultant potential and energy curves for the Au/SiC(111) interface. In particular, figure 2(b) demonstrates a check on the self-consistence of the inversion method. The AEs summarized by pair potentials (see formula (2)) present a good agreement with the original *ab initio* data. Thus, these pair potentials give a good description of the interface structures shown in figure 1.

Table 2 shows the potential parameters. They are in the Rahaman–Stillinger–Lemberg (RSL2) potential function form:

$$\phi(r_{ij}) = D_0 \mathrm{e}^{y(1-\frac{r_{ij}}{R_0})} + \frac{a_1}{1+\mathrm{e}^{b_1(r_{ij}-c_1)}} + \frac{a_2}{1+\mathrm{e}^{b_2(r_{ij}-c_2)}} + \frac{a_3}{1+\mathrm{e}^{b_3(r_{ij}-c_3)}}. \quad (12)$$

This form can describe well the pair interactions across interface.

2.2. Three-body term

As we have mentioned above, pair potentials are useful for top site structures (figure 2(b)). However, they do not perform so well for high energy structures, such as hollow site and hex site, as shown in figure 3. The AE checks are illustrated

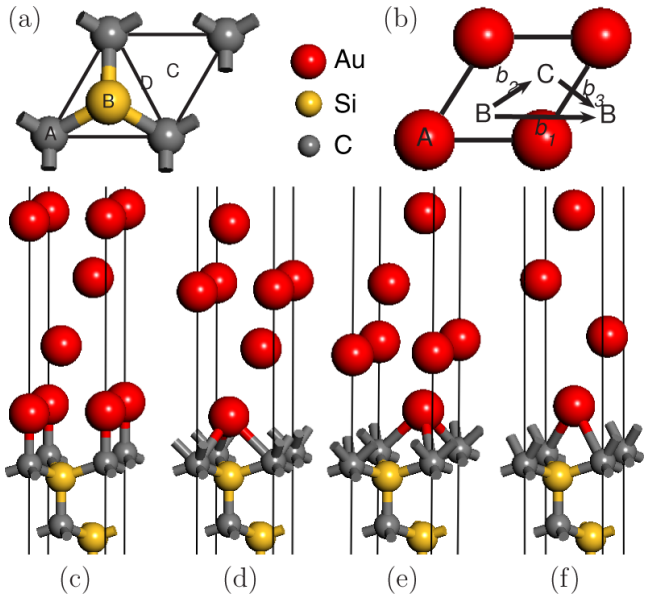

Figure 3. Atomic configurations of the metal(111)/SiC(111) interface. (a) SiC(111) surface (top view). The symbols A, B, C and D refer to top site, hollow site, hex site and bridge site, respectively. (c), (d), (e) and (f) are top site, hollow site, hex site and bridge site structures (side view), respectively. Taking the C-terminated Au/SiC case as an illustration, only a few layers near the interface are presented. (b) Metal(111) surface (top view) with Burgers vectors (presented in section 3.2) of a perfect dislocation $\boldsymbol{b}_1$ and partial dislocations $\boldsymbol{b}_2$, $\boldsymbol{b}_3$. Metal atoms are marked as A, B and C when they are, respectively, in the top site, hollow site and hex site according to the SiC(111) surface.

in figure 4. The disagreement between *ab initio* and pair-potential-calculated (RSL2) results are significant. Thus, three-body modification is required. For this purpose, the Stillinger–Weber three-body potential (SW3) [30, 31] is introduced as

$$\phi_{jik}(r_{ij}, r_{ik}, \theta_{jik}) = \lambda_{jik}\exp\left[\frac{\nu_{ij}}{r_{ij} - R_{ij}} + \frac{\nu_{ik}}{r_{ik} - R_{ik}}\right] \times (\cos\theta_{jik} - \cos\theta_0)^2, \quad (13)$$

where R_{ij} and R_{ik} are cutoff radii for atom pairs (i, j) and (i, k), respectively.

According to *ab initio* calculations [10], the interfacial charge transfer is mainly confined to the region between the first metal and SiC layers. The three-body interaction j–i–k is therefore limited to this region as well. As a result, some assumptions are needed to simplify the calculations. First, only six trimers are considered: M–C–Si, M–Si–C, M–C–M, M–Si–M, C–Si–C and Si–C–Si under the nearest-neighbor approximation. Second, the equilibrium angles θ_0 of M–C–Si and M–Si–C are set to 109.47°, which is equal to the bond angle of sp^3 hybridization. Third, trimers j–i–k, j–i–l and i–j–k share the same parameters ν_{ij} and R_{ij}.

The *ab initio* method is performed again to get AE curves for hollow and hex sites. Then, three-body potential parameters are derived from these curves by a fitting method. The results are listed in table 3. Figure 4 shows the transferability check for the hollow site and hex site. The *ab initio* AE data are well reproduced by considering two-body (RSL2) and three-body (SW3) interactions. It should be noted that the bridge site AE at the equilibrium point is also considered in the fitting procedure.

Table 3. Three-body potential parameters for metal(111)/SiC(111) interfaces.

j–i–k	λ_{jik} (eV)	θ_0 (deg)	ν_{ij} (Å)	ν_{ik} (Å)	R_{ij} (Å)	R_{ik} (Å)
Au–Si–C	0.8000	109.47	0.2300	0.2047	3.7500	3.1832
Au–Si–Au	2.2000	51.00	0.2300	0.2300	3.7500	3.7500
Au–C–Si	0.4250	109.47	0.2000	0.2047	3.5500	3.1832
Au–C–Au	2.8000	45.00	0.2000	0.2000	3.5500	3.5500
Ag–Si–C	0.3000	109.47	0.2000	0.2047	3.7500	3.1832
Ag–Si–Ag	1.1300	35.00	0.2000	0.2000	3.7500	3.7500
Ag–C–Si	0.1000	109.47	0.2700	0.2047	3.5500	3.1832
Ag–C–Ag	0.9000	5.00	0.2700	0.2700	3.5500	3.5500
Pt–Si–C	1.2500	109.47	0.2000	0.2047	3.5200	3.1832
Pt–Si–Pt	0.1500	30.00	0.2000	0.2000	3.5200	3.5200
Pt–C–Si	0.8500	109.47	0.2000	0.2047	3.4600	3.1832
Pt–C–Pt	0.6750	6.25	0.2000	0.2000	3.4600	3.4600
Al–Si–C [10]	0.9109	109.47	0.1878	0.2047	3.6500	3.1832
Al–Si–Al [10]	0.0342	180.00	0.1878	0.1878	3.6500	3.6500
Al–C–Si [10]	0.3283	109.47	0.0584	0.2047	3.4300	3.1832
Al–C–Al [10]	0.6229	2.30	0.0584	0.0584	3.4300	3.4300

Up to now, we have obtained all the terms of the interfacial potentials. The potentials inside metals and SiC can be cited from our previous works [16–21, 23]. For the SiC side, we adopt three-body potentials because the covalent Si–C bonds cannot be well described by pair potentials. For the metal side, the pair potentials can well reproduce the elastic constants c_{11} and c_{12}, so we think they are sufficient to study dislocations.

3. Dislocations

In this section, we study the dislocation structures in metal(111)/SiC(111) interfaces. Considering the effect of interfacial adhesion, we built two kinds of dislocation models, as shown in figure 5. The dislocation line (DL) is obtained by inserting an extra atomic layers in the metal slab. The Burgers vector is $\frac{1}{2}[1\bar{1}0]$ and DL is in the $[0\bar{1}1]$ direction. Under periodic boundary conditions, we have to introduce two variables: (i) a dislocation spacing (S) to describe the period of a dislocation model along its Burgers vector $\frac{1}{2}[1\bar{1}0]$, which is equal to the atom number of the first SiC layer in the dislocation model; and (ii) a dislocation position (P) to describe at which layer the dislocation appears. For example, $S = 10$, $P = 1$ in figure 5(a), and $S = 10$, $P = 2$ in figure 5(b). When the dislocation core appears at the interface plane ($P = 1$), the interface is the so-called semi-coherent structure with $S+1$:S atomic ratio between the first metal layer and the first SiC layer. Contrarily, if $P > 1$, the dislocation core appears in the metal slab and the atom ratio is 1:1 between the first metal and SiC layers. In this case, the interface is an ideal coherent one.

The models are relaxed by the energy minimization method. This method is implemented in the GULP program [32–34] until the relative energy change drops below 1×10^{-5} between two steps.

The thickness of the metal and SiC slabs should be selected with an appropriate value to avoid unexpected surface effects. For example, if the metal slab is extremely thin it can

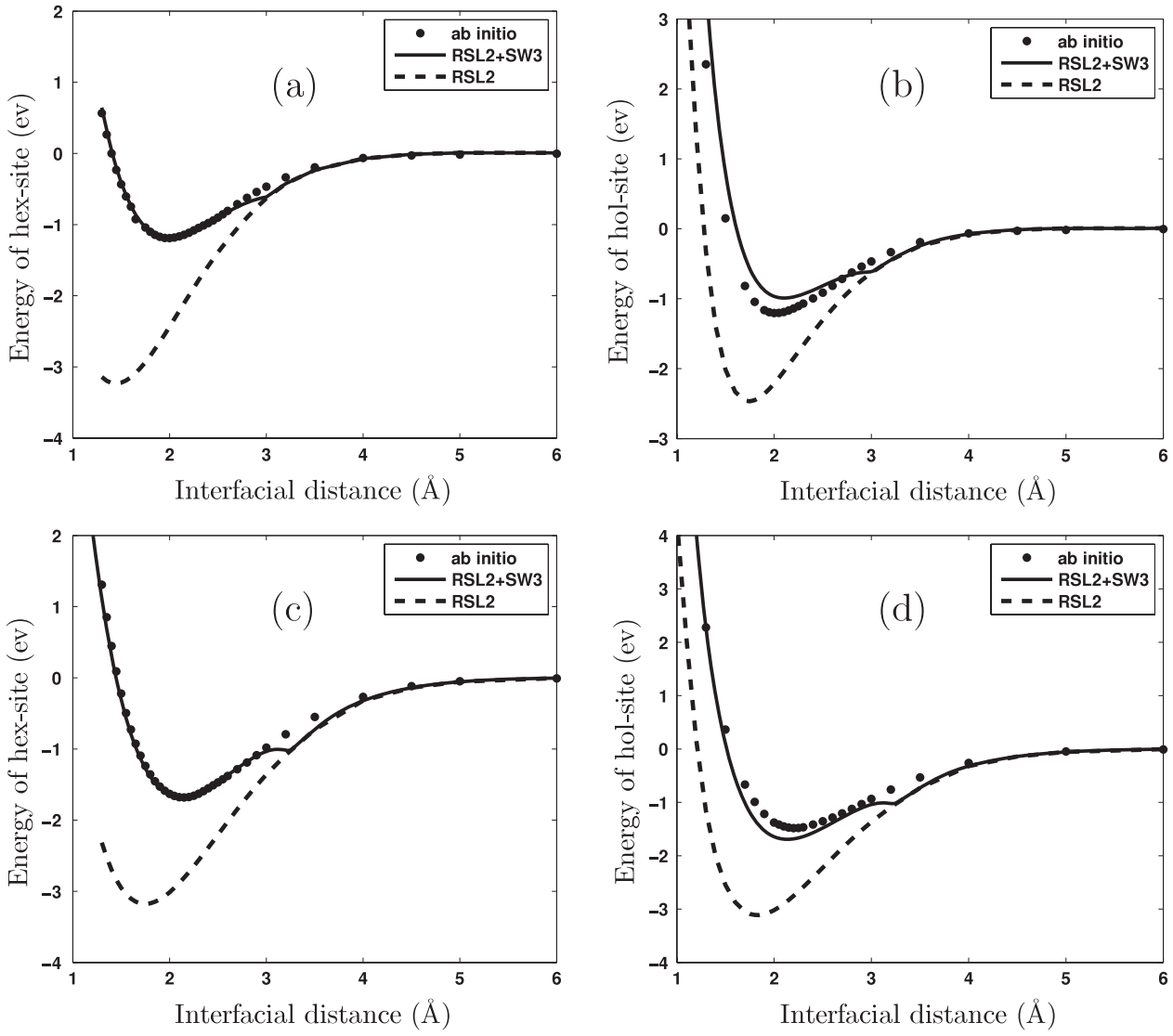

Figure 4. AE checks for hex site ((a) and (c)) and hollow site ((b) and (d)) Au/SiC(111) interfaces. (a) and (b) are C-terminated, (c) and (d) are Si-terminated. Scattered symbols, dashed lines and solid lines denote AE data derived from *ab initio*, two-body potential (RSL2), and two- and three-body potential calculations (RSL2 + SW3), respectively. The bridge site AE is just fitted at the equilibrium point, so is not presented here.

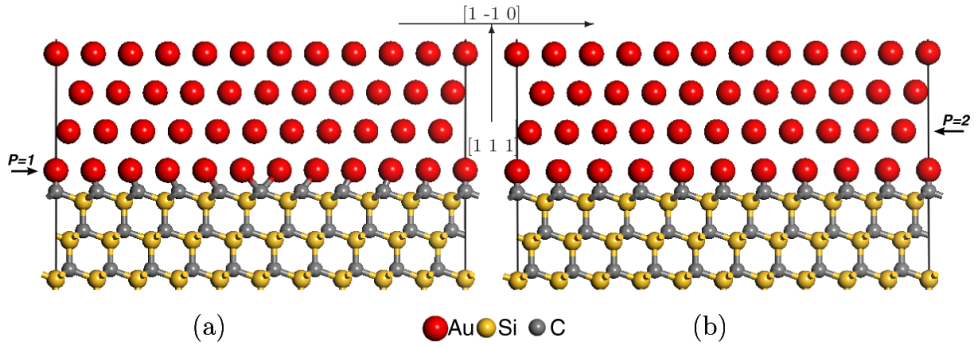

Figure 5. Two initial dislocation models of C-terminated Au(111)/SiC(111) interfaces (side view). The dislocation core is positioned: (a) at the first metal layer ($P = 1$), (b) at the second metal layer ($P = 2$).

not be used in a film–substrate system with dislocation. For this purpose, we relax the ideal C-terminated Au(111)/SiC(111) interface model to analyze its interfacial distance, as shown in figure 6. According to the check, the interfacial distance remains to constant when the number of metal layers is greater than six. Thus, we built the initial dislocation

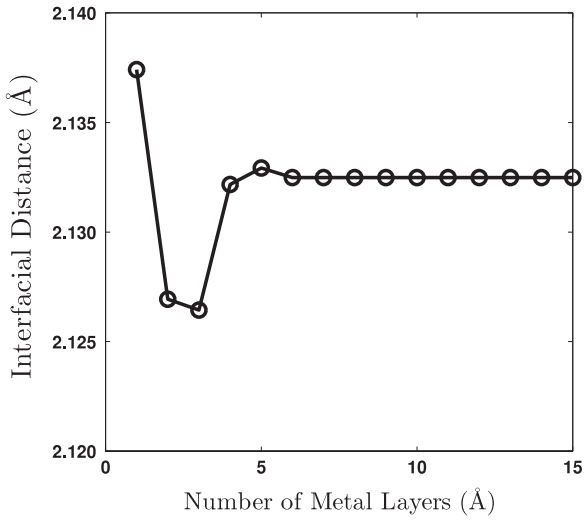

Figure 6. Thickness check in C-terminated Au(111)/SiC(111) interfaces (relaxed by potentials).

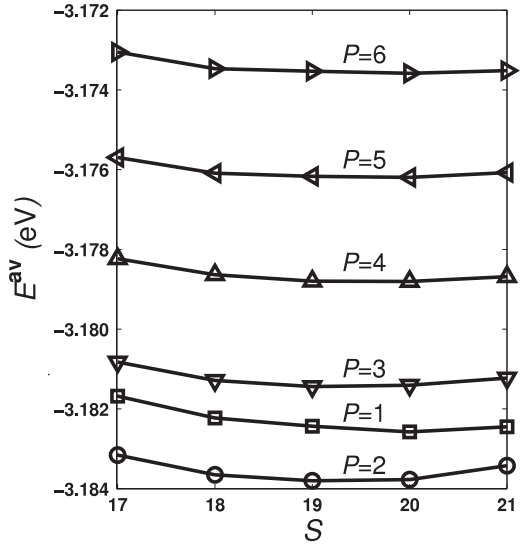

Figure 7. Dislocation spacing and position (S–P) selection for the C-terminated Au(111)/SiC(111) interface as an illustration. The minimum has $P = 2$, indicating that the dislocation appears in the second metal layer.

models with fifteen metal MLs and twelve SiC MLs, and the bottommost four SiC MLs are fixed to simulate the bulk lattice. Additionally, the vacuum gap is chosen as 20 Å.

3.1. DL's spacing and position

As a criterion for spacing and position (S–P) selection, the average metal energy is defined as

$$E^{av} = \frac{E^{tt} - E^{SiC}}{N}, \tag{14}$$

where N denotes the number of metal atoms, and E^{tt} and E^{SiC} are the energies of relaxed interface and SiC slabs, respectively, calculated by interatomic potentials. Figure 7 shows the

Table 4. Parameters for metal(111)/SiC(111) interfacial dislocations. S, P, and E^{av} are derived from the S–P selections in section 3.1. For comparison, S_0 is derived from the geometric match and E^{bk} is the cohesive energy of the bulk metal. E^{br}, E^{st} and δ are defined in section 3.3. Energies are in units of eV.

	S_0	S	P	E^{av}	E^{bk}	E^{br}	E^{st}	δ
$Au/(SiC)_C$	22.6	19	2	−3.1838	−3.2483	0.43	0.69	0.62
$Au/(SiC)_{Si}$	22.6	20	2	−3.2309	−3.2483	0.29	0.71	0.41
$Al/(SiC)_C$	11.3	10	3	−3.3646	−3.5056	0.60	0.62	0.97
$Al/(SiC)_{Si}$	11.3	10	2	−3.3494	−3.5056	0.33	0.62	0.53
$Pt/(SiC)_C$	10.6	9	1	−5.5816	−5.8647	0.78	2.22	0.35
$Pt/(SiC)_{Si}$	10.6	9	1	−5.6090	−5.8647	0.29	2.22	0.13
$Ag/(SiC)_C$	17.5	16	1	−2.8117	−2.9093	0.09	0.70	0.13
$Ag/(SiC)_{Si}$	17.5	15	1	−2.8449	−2.9093	0.04	0.66	0.06

average metal energy E^{av} of different S–P combinations for the C-terminated Au(111)/SiC(111) interface. We calculated the E^{av} of thirty S–P combinations. For a certain S, the dislocation core appears in the second metal layers ($P = 2$). The most stable case is $S = 19$ and $P = 2$ for C-terminated Au(111)/SiC(111) interfaces. All the results of S–P selection are shown in table 4. There are two kinds of dislocation in the M(111)/SiC(111) interfaces. For M = (Ag, Pt), the dislocation core appears in the first metal layer ($P = 1$). For M = (Au, Al), the dislocation core appears in metal slabs ($P > 1$). The structural difference is shown in detail in section 3.2. For comparison, we also present the ideal DL spacing determined by geometric matching:

$$S_0 = \frac{1}{\gamma}, \tag{15}$$

where γ is the interfacial mismatch. Likewise, the cohesive energy of bulk metal (E^{bk}) is also presented. It is also calculated from interatomic potentials.

3.2. Atom distribution

Next, we present the possibility of dislocation decomposition beyond the S–P selection. To do this, we are going to investigate the atomic distributions of potential-relaxed dislocation models.

3.2.1. M(111)/SiC(111) (M = Au, Al). As is well known, the fcc lattice is a kind of close-packed structure. Its atomic arrangement order is A–B–C along the [111] direction, where A, B and C are three MLs in specific position relations in the bulk metal. For the metal(111)/SiC(111) interface, we redefine symbols A, B, C and D to denote metal layers on the top site, hollow site, hex site and bridge site respectively, as illustrated in figure 3.

In order to display the detailed atomic arrangements of M(111)/SiC(111) M = (Au, Al) dislocations, the Si-terminated Au(111)/SiC(111) interface is shown in figure 8. To present the dislocation core clearly, the first and the second Au MLs are colored red and green respectively. This model is found in spacing and position selections with $S = 20$ and $P = 2$. In this case, the dislocation cores appear in the second metal layer. The first metal layer (top site) is coherent with the

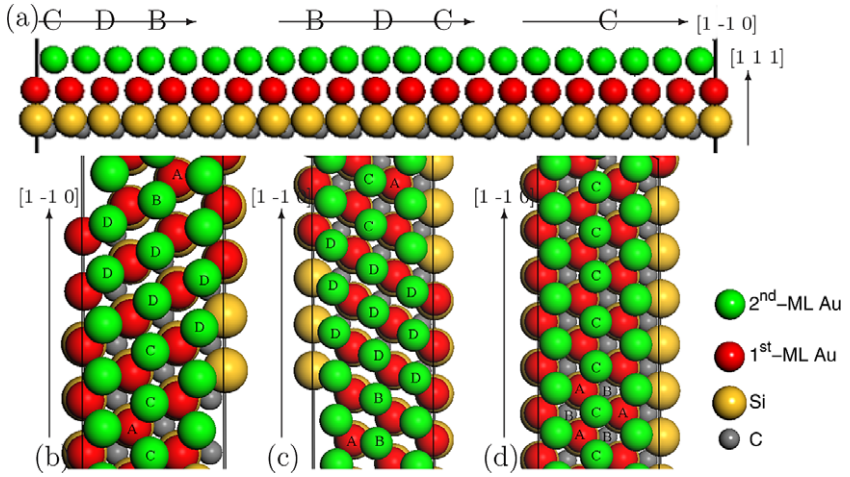

Figure 8. Dislocation structure in the Si-terminated Au(111)/SiC(111) interface. (a) is a side view, (b), (c) and (d) are top views corresponding to three parts denoted C–D–B, B–D–C, C in (a), respectively. Only the second Au ML and the first Au/Si/C MLs are presented. The core of partial dislocation (region-D) appears in the second Au layer. Region-C is the stacking fault between two partial dislocations.

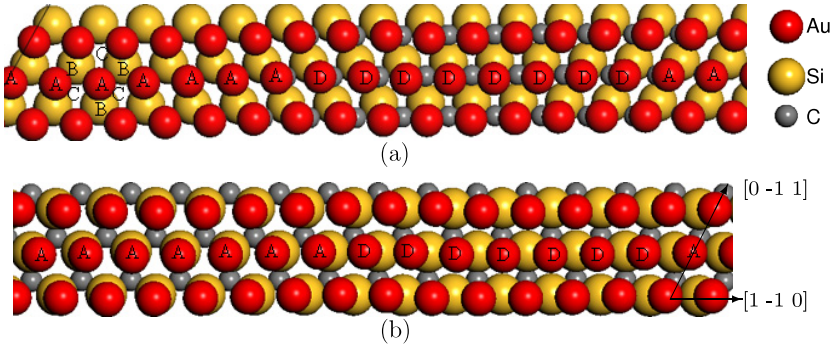

Figure 9. Dislocation structures in Ag(111)/SiC(111) interfaces (top view). (a) C-terminated, (b) Si-terminated. Only the first Ag/Si/C MLs are presented. The core of perfect dislocation (region-D) appears in the first metal layer.

SiC surface. As a result of one extra gold atom in the second metal layer, some atoms originally on the hollow site (B) will gradually move to the hex site (C). It should be noted that this motion is a kind of collective behavior. Thus, we can deem that a perfect dislocation decomposes into two partial dislocations (also named imperfect dislocations), which is similar to the phenomenon appearing in metal bulk materials [35–37]. In figure 8, region-D is the core of partial dislocation and region-C is the stacking fault between two partial dislocations. In this condition, the resultant dislocation decomposition formula is

$$\tfrac{1}{2}[1\bar{1}0] \longrightarrow \tfrac{1}{6}[1\bar{2}1] + \tfrac{1}{6}[2\bar{1}\bar{1}], \qquad (16)$$

where $\frac{1}{2}[1\bar{1}0]$ ($\boldsymbol{b}_1$), $\frac{1}{6}[1\bar{2}1]$ ($\boldsymbol{b}_2$) and $\frac{1}{6}[2\bar{1}\bar{1}]$ ($\boldsymbol{b}_3$) are illustrated in figure 3(b).

3.2.2. M(111)/SiC(111) (M = Ag, Pt). Different from M(111)/SiC(111) (M = Au, Al), M(111)/SiC(111) (M = Ag, Pt) interfaces have $P = 1$. The case of silver is illustrated in figure 9. The first metal layer consists of a top site (A) and bridge site (D), where region-A, presented as a coherent area, is the main part, and region-D, presented as a dislocation core, is the small part. This feature implies that the perfect dislocation does not decompose and its Burgers vector is still $\frac{1}{2}[1\bar{1}0]$ after relaxation. The result for Pt/SiC is similar to Ag/SiC, so is not presented again.

Next, the influence of interfacial structure on electronic properties is discussed. Coherent interface models are available for M(111)/SiC(111) M = (Au, Al) because the dislocations appear in the metal slab as simulated by potentials. The coherent interlayer keeps the interfacial configuration homogeneous in the top site. So the misfit dislocation is weakly related to the interfacial electronic structure, as it is above the interlayer. In many *ab initio* works, the ideal coherent interface is a general approximation for the study of electronic properties. However, in a semi-coherent interface such as Ag(111)/SiC(111), some metal atoms at the interface plane are located at the high energy site. Hence we should consider the change of interfacial electronic properties determined by dislocations in this kind of interface.

3.3. Energy distribution

In general, the dislocation position of a film–substrate system is determined by two factors in the energetic view. One is the interfacial adhesion, which ejects the dislocation core into the metal side. The other is the misfit-induced strain energy in

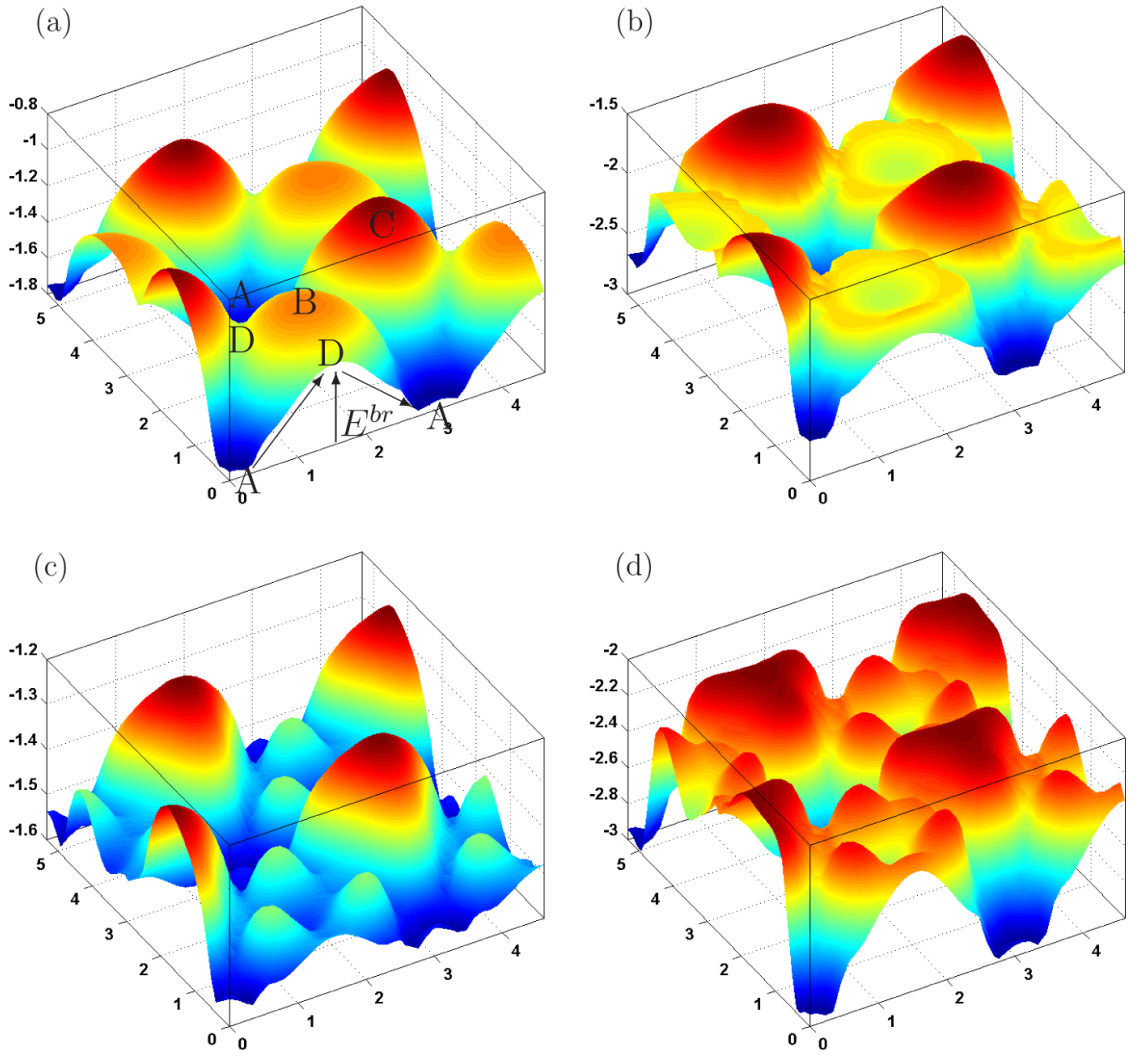

Figure 10. C-terminated AE distribution of metal(111)/SiC(111) interfaces. Parallel to interface, the x-axis is vector $\frac{3}{2}[1\bar{1}0]$ and the y-axis is $[\bar{1}\bar{1}2]$ (units: Å). The z-axis represents the AE (units: eV/unitcell). In (a), the definition of the energy barrier $E^{\rm br}$ is presented. Symbols A, B, C, D denote when the metal slab is positioned at the top site, hollow site, hex site and bridge site, respectively. (a) Au(111)/SiC(111), (b) Al(111)/SiC(111), (c) Ag(111)/SiC(111) and (d) Pt(111)/SiC(111).

the metal film. In this condition, we investigate the relative strengths of the interfacial adhesion and strain energy.

For this purpose, we calculate AE distributions around the SiC(111) surface first. The corresponding models are shown in figure 3. Each model consists of fifteen metal MLs and twelve SiC MLs. To get AEs at all the points on SiC, we fix four SiC MLs on the bottom and move the whole metal slab to a point (x, y). In each relaxation process, variables x and y (parallel to interface) are fixed and variable z (vertical to interface) is free. By this method, we obtain all the AE distributions for Au, Ag, Al and Pt, as shown in figures 10 and 11. The top site is stable for metal slabs on SiC(111) surfaces. If a dislocation core appears in the first metal layer, some atoms will deviate from this equilibrium position. The collective gradual regions are displayed in figure 9. The gradual path is from the top site (A) to the bridge site (D), and then to the next top site (A). Thus, we use the barrier energy ($E^{\rm br}$) along this path to evaluate the interfacial effect. The calculation of $E^{\rm br}$ is shown in figure 10(a).

Now, let us consider the strain energy $E^{\rm st}$ induced by the interfacial misfit. We are going to study some empirical relations between $E^{\rm av}$ based on figure 7. For the case of $S = 19$, $E_3^{\rm av} - E_4^{\rm av} \approx E_4^{\rm av} - E_5^{\rm av} \approx E_5^{\rm av} - E_6^{\rm av} \approx \cdots$, where $E_P^{\rm av}$ denotes the average metal energy when the dislocation appears in the Pth layer. By formula (14), this relation is approximately written as

$$\frac{E_3^{\rm tt} - E^{\rm SiC}}{N_3} - \frac{E_4^{\rm tt} - E^{\rm SiC}}{N_4} = \frac{E_4^{\rm tt} - E^{\rm SiC}}{N_4} - \frac{E_5^{\rm tt} - E^{\rm SiC}}{N_5} = \frac{E_5^{\rm tt} - E^{\rm SiC}}{N_5} - \frac{E_6^{\rm tt} - E^{\rm SiC}}{N_6} = \cdots. \tag{17}$$

Taking the C-terminated Au(111)/SiC(111) case as an illustration, $N_3 = 298$, $N_4 = 297$, and $N_5 = 296$. As a result, N_4 and N_5 are approximately equal to N_3. The change in total energy by varying the subscript from $P + 1$ to P is

$$E_P^{\rm tt} - E_{P+1}^{\rm tt} = E^{\rm bk} - E^{\rm st} \tag{18}$$

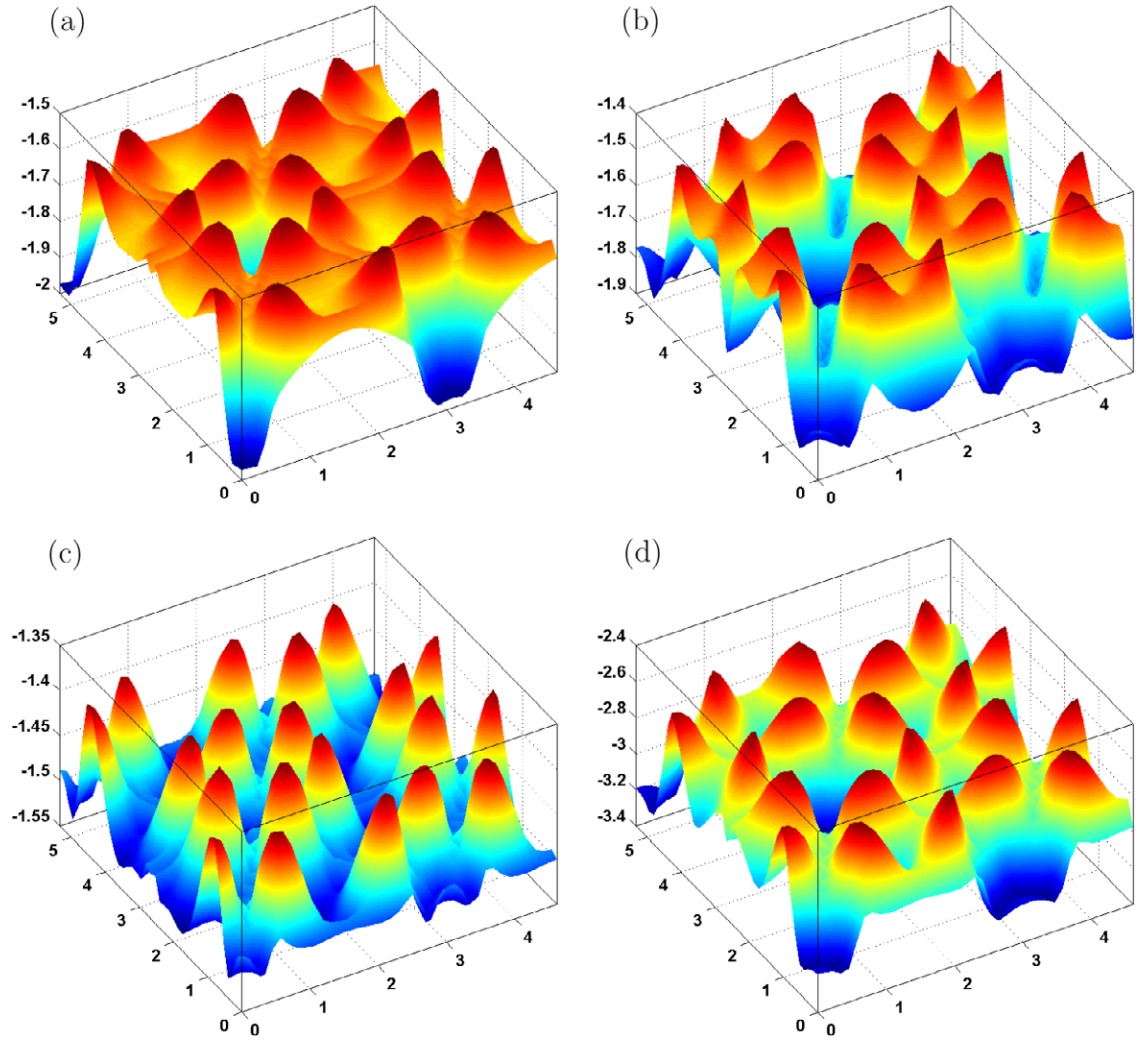

Figure 11. Si-terminated AE distribution of metal(111)/SiC(111) interfaces. Parallel to the interface, the x-axis is vector $\frac{3}{2}[1\bar{1}0]$ and the y-axis is $[\bar{1}\bar{1}2]$ (units: Å). The z-axis represents the AE (units: eV/unitcell). (a) Au(111)/SiC(111), (b) Al(111)/SiC(111), (c) Ag(111)/SiC(111) and (d) Pt(111)/SiC(111) interface.

where E^{st} denotes the misfit-induced strain energy by decreasing one metal atom. Substituting (18) into (17) and replacing N_{p+m} by N_p, we get

$$E^{\mathrm{st}} = N_P(E^{\mathrm{av}}_{P+m} - E^{\mathrm{av}}_P)/m, \tag{19}$$

where P should be greater than two to avoid an interfacial effect. In this work, we adopt $p = 4$, $m = 4$ to calculate E^{st}. For comparison, we define the ratio between E^{br} and E^{st} as

$$\delta = \frac{E^{\mathrm{br}}}{E^{\mathrm{st}}}. \tag{20}$$

Data of E^{br}, E^{st} and δ are listed in table 4. The δ of the M(111)/SiC(111) (M = Au, Al) interface is greater than that of the M(111)/SiC(111) (M = Ag, Pt) interface. It shows good agreement with position selections in section 3.1 that dislocations appear in the metal slab for Au and Al and at the interface plane for Ag and Pt. It should be noted that the Ag–SiC system forms a semi-coherent interface because of the weak interfacial effect ($E^{\mathrm{br}} < 0.1$ eV), while the Pt–SiC system does the same because of the strong misfit-induced strain energy ($E^{\mathrm{st}} = 1.22$ eV).

4. Conclusion and discussion

In conclusion, we develop a series of interfacial potentials for M(111)/SiC(111) (M = Au, Ag, Al, Pt) interfaces and use them to study the misfit dislocation structures. The calculation shows that the dislocation core appears in the first metal layer for the M(111)/SiC(111) (M = Ag, Pt) interface. The corresponding misfit dislocation is 60° perfect dislocation. Contrarily, the dislocation core appears in the second or third metal layers for the M(111)/SiC(111) (M = Au, Al) interface. In this case, a perfect dislocation decomposes into two partial dislocations. One is a 90° edge dislocation and the other is a 30° mixed dislocation. These partial dislocations induce stacking-fault regions in the metal film.

In most previous *ab initio* works, there are only ideal and coherent metal/SiC interface models. According to

our potential-relaxed results, this agrees with the case of M(111)/SiC(111) (M = Au, Al) interfaces that the dislocation core appears inside the metal film and the interface is coherent. However, in the case of M(111)/SiC(111) (M = Ag, Pt), the dislocation core appears in the first metal layer. The first-layer metal atoms are distributed in different positions such that some atoms are located at the top site and others at the bridge site. This is a semi-coherent interface. For further study, we will consider the influence of a semi-coherent interface on interfacial adhesion and electronic properties.

Acknowledgments

This work is supported by the Nature Science Foundation of China (NSFC), No. 50531050, and 973 project, No. 2006CB605100. The authors would like to thank M Kohyama for his helpful suggestions and discussion.

References

[1] Aboelfotoh M O 2003 *Phys. Rev.* B **67** 075312
[2] Zhen L X, Xie M H and Tong S Y 2000 *Phys. Rev.* B **61** 4890
[3] Kubo O *et al* 2004 *Phys. Rev.* B **69** 045406
[4] Kohyama M and Hoekstra J 2000 *Phys. Rev.* B **61** 2672
[5] Miao M S *et al* 2002 *Phys. Rev.* B **66** 064107
[6] Rao B K and Jena P 1990 *Appl. Phys. Lett.* **57** 2308
[7] Luo X, Qian G F and Wang E G 1999 *Phys. Rev.* B **59** 10125
[8] Ito T, Khor K E and Das Sarma S 1990 *Phys. Rev.* B **41** 3893
[9] Zhao H Y and Chen N X 2008 *Inverse Problems* **24** 035019
[10] Zhao H Y, Chen N X and Long Y 2009 *J. Phys.: Condens. Matter* **21** 225002
[11] Chen N X 1990 *Phys. Rev. Lett.* **64** 1193
[12] Vogelsang M, Arsenault R J and Fisher R M 1986 *Metall. Trans.* A **17A** 380
[13] Komninou P *et al* 1999 *J. Cryst. Growth* **203** 103
[14] Ovid'Ko I A and Sheinerman A G 2008 *Phys. Rev.* B **77** 054109
[15] Mizoguchi T *et al* 2006 *Phys. Rev.* B **74** 235408
[16] Xie Q and Chen N X 1995 *Phys. Rev.* B **51** 15856
[17] Chen N X, Chen Z D and Wei Y C 1997 *Phys. Rev.* E **55** R5–8
[18] Chen N X *et al* 1998 *Phys. Rev.* B **57** 14203
[19] Chen N X, Shen J and Su X P 2001 *J. Phys.: Condens. Matter* **13** 2727
[20] Zhang S and Chen N X 2002 *Phys. Rev.* B **66** 64106
[21] Long Y, Chen N X and Zhang W Q 2005 *J. Phys.: Condens. Matter* **17** 2045
[22] Long Y, Chen N X and Wang H Y 2005 *J. Phys.: Condens. Matter* **17** 6149
[23] Long Y and Chen N X 2007 *J. Phys.: Condens. Matter* **19** 196216
[24] Long Y and Chen N X 2008 *J. Phys.: Condens. Matter* **20** 135005
[25] Payne M C *et al* 1992 *Rev. Mod. Phys.* **64** 1045
[26] Milman V *et al* 2000 *Int. J. Quantum Chem.* **77** 895
[27] Segall M D *et al* 2002 *J. Phys.: Condens. Matter* **14** 2717
[28] Monkhorst H J and Pack J D 1976 *Phys. Rev.* B **13** 5188
[29] MacDonald A H 1978 *Phys. Rev.* B **18** 5897
[30] Stillinger F H and Weber T A 1985 *Phys. Rev.* B **31** 5262
[31] Feuston B P and Garofalini S H 1988 *J. Chem. Phys.* **89** 5818
[32] Gale J D 1997 *J. Chem. Soc. Faraday Trans.* **1** 629
[33] Gale J D 1998 *J. Phys. Chem.* B **102** 5423
[34] Gale J D and Rohl A L 2003 *Mol. Simul.* **29** 291
[35] Meyers M A and Chawla K K 1998 *Mechanical Behavior of Materials* (Englewood Cliffs, NJ: Prentice-Hall)
[36] Byun T S 2003 *Acta Mater.* **51** 3063
[37] Liao X Z *et al* 2003 *Appl. Phys. Lett.* **83** 632